

---

# Learning to Have an Ear for Face Super-Resolution

---

**Givi Meishvili**      **Simon Jenni**      **Paolo Favaro**  
University of Bern      University of Bern      University of Bern  
Bern 3012              Bern 3012              Bern 3012  
{givi.meishvili, simon.jenni, paolo.favaro}@inf.unibe.ch

## Abstract

We propose a novel method to perform extreme (16x) face super-resolution by exploiting audio. Super-resolution is the task of recovering a high-resolution image from a low-resolution one. When the resolution of the input image is too low (e.g.,  $8 \times 8$  pixels), the loss of information is so dire that the details of the original identity have been lost. However, when the low-resolution image is extracted from a video, the audio track is also available. Because the audio carries information about the face identity, we propose to exploit it in the face reconstruction process. Towards this goal, we propose a model and a training procedure to extract information about the identity of a person from her audio track and to combine it with the information extracted from the low-resolution input image, which relates more to pose and colors of the face. We demonstrate that the combination of these two inputs yields high-resolution images that better capture the correct identity of the face. In particular, we show that audio can assist in recovering attributes such as the gender and the identity, and thus improve the correctness of the image reconstruction process. Our procedure does not make use of human annotation and thus can be easily trained with existing video datasets. Moreover, we show that our model allows one to mix low-resolution images and audio from different videos and to generate realistic faces with semantically meaningful combinations.

## 1 Introduction

Image super-resolution is the task of recovering details of an image that has been degraded through a spatial quantization process. A formulation of this problem is to define a (low) source and a (high) target resolution, which are related by a fixed scaling factor. Typical scaling factors are in the order of  $4 \times$  or  $8 \times$  increase of resolution from the input to the output. For these factors the restoration task is close to a sharpening problem and the focus is more on recovering small structures such as edges and corners or even small texture patches. In the more extreme case where the scaling factor is  $16 \times$  or above, the loss of detail is so considerable that important semantic information might be lost. This is the case, for example, of images of faces at the  $8 \times 8$  pixels resolution, where information about the original identity of the person is no longer available (see, for example, the low-resolution input in Fig. 1). What is left is the viewpoint and colors of the face, clothing and the background. While it is possible to hallucinate plausible high-resolution images from such limited information, it would be difficult to correctly recover useful attributes such as the gender or even the identity.

If the low-resolution image of a face is extracted from a video, we might also have access to the audio of that person. Despite the very different nature of aural and visual signals, they both capture some shared attributes of a person and, in particular, her identity. In fact, when we hear the voice of an iconic actor we can often picture his or her face in our mind. What is more remarkable is that we can even match the looks of a person we have not met with their sound (see Smith et al. [2016]). While this aural-visual redundancy may be a benefit to social communication, it can also be a benefit to image processing and, in particular, image super-resolution. Therefore, we propose to build a model

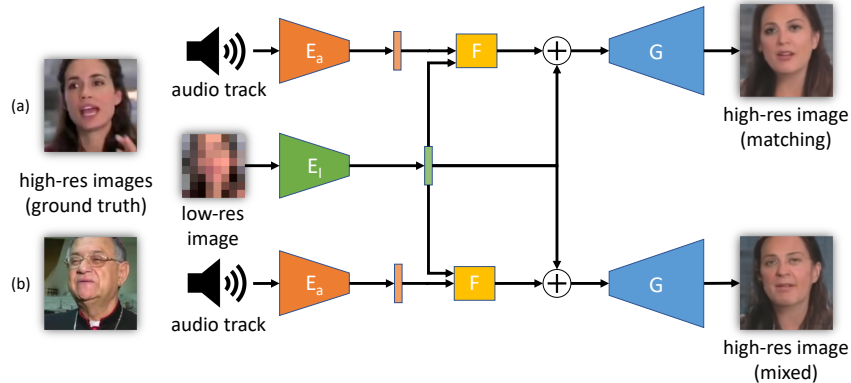


Figure 1: Simplified scheme of the proposed model. The model can be used (a) with matching inputs or (b) by mixing low-resolution images with audios from other videos. The low-resolution image ( $8 \times 8$  pixels) is fed to an encoder  $E_l$  to obtain an intermediate latent representation. A residual is computed by fusing in the network  $F$  the encoded audio track (through the encoder  $E_a$ ) with the encoded low-resolution image. The residual is used to update the latent representation of the low-resolution image and then produce the high-resolution image through the generator  $G$ .

for face super-resolution by exploiting both a low-resolution image and its audio. To the best of our knowledge, this has never been explored before.

A natural way to solve this task is to build a model with two encoding networks, one for the low-resolution image and one for the audio, and a decoding network mapping the concatenation of the encoders output to a high resolution image. Unfortunately, we found experimentally that the joint training of these networks leads to a degenerate solution, where the audio encoder learns to ignore its input. We conjecture that this is due to the different nature of the aural and visual signals, which corresponds to a different level of difficulty in disentangling their information to a common latent space. Thus, it might be easier for the training algorithm to overfit on the training set with the low-resolution images, than to exploit the audio input. To address this conjecture, we propose to train the low-resolution image encoder and the audio encoder separately, so that their disentanglement accuracy can be equalized.

To this aim, we first train a generator  $G$  that starts from a Gaussian latent space and outputs high resolution images (see Fig. 1). The generator is trained as in the recent StyleGAN of Karras et al. [2018], which produces very high quality samples and a hierarchical structure of the latent space. Then, we train a reference encoder to invert the generator by using an autoencoding constraint. The reference encoder maps a high-resolution image to the latent space of the generator, which then outputs an approximation of the input image. Then, given a matching high/low-resolution image pair, we pre-train a low-resolution image encoder  $E_l$  to map its input to the same latent representation of the reference encoder (on the high-resolution image). As a second step, we train an audio encoder  $E_a$  and a fusion network  $F$  to improve the latent representation of the (fixed) low-resolution image encoder  $E_l$ . To speed up the training of the audio encoder we also pre-train it by using as latent representation the average of the outputs of the reference encoder on a high-resolution image and its horizontally mirrored version (this averaging removes information, such as the viewpoint, that the audio cannot carry). In Section 3, we describe in detail the training of each of the above models. Finally, in Section 4 we demonstrate experimentally that the proposed architecture and training procedure successfully fuses aural and visual data. We show that the fusion yields high resolution images with more accurate identities and gender attributes than the reconstruction based on the lone low-resolution image. We also show that the fusion is semantically meaningful by mixing low-resolution images and audio from different videos (see an example in Fig. 1 (b)).

## 2 Related Work

**General Super-Resolution.** Advances in general super-resolution have been largely driven by the introduction of task-specific network architectures and components. Examples are: Residual Dense Networks (Zhang et al. [2018c]), Multi-scale Residual Networks (Li et al. [2018]), lightweight

Cascading Residual Networks (Ahn et al. [2018]), Deep Recursive Residual Networks (Tai et al. [2017]), Deep Residual Channel Attention Networks (Zhang et al. [2018b]), Information Distillation Networks (Hui et al. [2018]), Spatial Feature Transformer layers (Wang et al. [2018]), Deep Back-Projection Networks (Haris et al. [2018]), Dual-State Recurrent Networks (Han et al. [2018]), and the Laplacian Pyramid Super-Resolution Networks (Lai et al. [2017]). In our method, we do not rely on task-specific architectures, although we leverage the design of a state-of-the-art generative model (Karras et al. [2018]). Many general super-resolution methods also make use of adversarial training. Ledig et al. [2017] presented SRGAN, a generative adversarial network for image super-resolution. Park et al. [2018] suggested a GAN based super-resolution method with an additional feature discriminator. Bulat et al. [2018] trained a GAN to learn the true image degradation model (high-to-low) and used it to train another low-to-high GAN. While we also make use of a GAN, our approach is quite different from those works since we pre-train and fix the generator of the GAN.

**Face Super-Resolution.** The face super-resolution problem has attracted a lot of attention in recent years. Several methods were proposed that tackle the problem with additional supervision and multi-task learning. Bulat and Tzimiropoulos [2018] proposed Super-FAN, a method that addresses both face super-resolution and landmark detection in a multi-task fashion. Yu et al. [2018a] tied super-resolution to a facial component heatmap estimation. Chen et al. [2018] incorporated facial landmark heatmaps and parsing maps as a facial geometry prior. Zhang et al. [2018a] improved the recognizability of ultra-low-resolution faces using identity information in an identity loss that measures the identity difference between a hallucinated face and its high-resolution counterpart. Yu et al. [2018b] proposed an attribute guided upsampling CNN to reduce the ambiguity of one-to-many mappings in the case of  $8\times$  super-resolution. In contrast, by using videos with corresponding audio tracks our method does not rely on additional human annotation. Several face super-resolution models rely on the use of GANs to produce realistic high-resolution outputs (Bulat and Tzimiropoulos [2018], Chen et al. [2018], Yu et al. [2018b]). Xu et al. [2017] adopted a GAN to learn a category-specific prior for face super-resolution. Our work also relies on the use of a GAN to learn a face specific prior. Our model is more general however since it provides a one-to-many mapping through the conditioning on the audio.

**Usage of Audio in Vision Tasks.** The usage of audio in combination with video has received a lot of attention recently. Zhou et al. [2018] trained a CNN to directly predict the raw audio waveform from a sequence of video frames. Shlizerman et al. [2018] showed that class specific natural body dynamics can be predicted from an audio signal. Arandjelovic and Zisserman [2018] tackled the audio-video correspondence task and demonstrated the capability to localize semantic objects within an image based on audio. Owens and Efros [2018] additionally achieved on/off-screen audio source separation. Sterling et al. [2018] presented a multimodal neural network optimized for estimating an object’s geometry and material. Zhao et al. [2018] introduced PixelPlayer, a system that learns to separate the input sounds into a set of components that represent the sound from each pixel. Two recent works proposed visually-aided audio source separation frameworks (Gao et al. [2018], Ephrat et al. [2018]). Tian et al. [2018] addressed the problem of Audio-Visual Event localization. Some works tackled the problem of generating talking faces based on an input face image and an audio signal (Song et al. [2018], Zhu et al. [2018]). To the best of our knowledge we are the first to use audio in an image restoration task.

### 3 Using Audio for Face Super-Resolution

Our goal is to design a model that is able to generate high resolution images based on a low resolution input image and an additional audio signal. The dataset is therefore given by  $\mathcal{D} = \{(x_i^h, x_i^l, a_i) \mid i = 1, \dots, n\}$  where  $x_i^h$  is the high-resolution image,  $x_i^l$  is the low-resolution image and  $a_i$  is a corresponding audio signal. Our model consists of several components: a low-resolution encoder  $E_l$ , an audio encoder  $E_a$ , a fusion network  $F$  and a face generator  $G$ . An overview of the complete architecture is given in Fig. 1.

#### 3.1 Disentangling Representations of Aural and Visual Signals

As mentioned in the introduction, a natural choice to solve our task is to train a feedforward network to match the ground truth high resolution image given its low-resolution image and audio signal. Experimentally, we found that such a system tends to ignore the audio signal and to yield a one-to-one

mapping from a low-resolution to a single high-resolution image. We believe that this problem is due to the different nature of the aural and visual signals, and the choice of the structure of the latent space. The fusion of both signals requires disentangling their information to a common latent space through the encoders. However, the audio signal seems to require longer processing and more network capacity to convert it to the latent space. This conversion can also be aggravated by the structure of the latent space, which might be biased more towards images than audio. Ideally, the low-resolution image should only condition the feedforward network to produce the most likely corresponding high-resolution output and the audio signal should introduce some local variation (i.e., modifying the gender or the age of the output). Therefore, for the fusion to be effective it would be useful if the audio could act on some fixed intermediate representation from the low-resolution image, where face attributes present in the audio are disentangled.

For these reasons we opted to pre-train and fix the decoder network as the generator of a StyleGAN (Karras et al. [2018]). This model has been shown to produce realistic high resolution images along with a good disentanglement of the factors of variation in the intermediate representations. Such a model should therefore act as a good prior for generating high resolution face images and the disentangled intermediate representations should allow better editing based on the audio signal. Formally, we learn a generative model of face images  $G(z)$  where  $z \sim \mathcal{N}(0, I_d)$  by optimizing the default non-saturating loss function of the StyleGAN (see Karras et al. [2018] for details).

### 3.2 Inverting the Generator

The task of regressing the high-resolution images directly can be translated into mapping them to the latent representation that, when fed to the generator network, results in the original high-resolution images. Our goal is that the fusion of the information provided by the low-resolution image and audio track will result in a reconstruction that is close to the original high resolution image. We therefore want to find suitable targets  $z_i$  for the training of our model. To this end, we train a high-resolution image encoder  $E_h$  by minimizing

$$\min_{E_h} \sum_{i=1}^n \ell_{feat}(G(E_h(x_i^h)), x_i^h), \quad (1)$$

where  $\ell_{feat}$  is a perceptual loss based on VGG16 features (see Supplementary material for more details). We found that regressing a single  $z_i = E_h(x_i^h)$  is not sufficient to recover a good approximation of  $x_i^h$ . In the style-based generator each  $z$  is mapped to a vector  $w$ , which is then replicated and inserted at  $k$  different layers of the generator (each corresponding to different image scales). To improve the high-resolution reconstruction, we instead generate  $k$  different  $z_j$ ,  $j = 1, \dots, k$ , and feed the resulting  $w_j$  to the corresponding layers in the generator. The output of  $E_h$  therefore lies in  $\mathbb{R}^{k \times d}$ . Note that this is not too dissimilar from the training of the style-based generator, where the  $w$ -s of different images are randomly mixed at different scales.

### 3.3 Pre-Training Low-Resolution and Audio Encoders

Given the high-resolution image encoder, we now have target outputs for the low-resolution and audio fusion. However, the training of a fusion model directly on these targets runs into some difficulties. As mentioned before, we find experimentally that, given enough capacity, a fusion model  $F(x_i^l, a_i)$  learns to predict  $E_h(x_i^h)$  well, while ignoring the audio signal  $a_i$  almost completely. To address this degenerate behavior, we train the two encoders  $E_l$  and  $E_a$  separately to extract as much information from the two modalities as possible and only later fuse them. To ensure that neither of the two encoders can overfit the whole training set we partition it into two sets:  $\mathcal{D}_1 = \{(x_i^h, x_i^l, a_i) \mid i = 1, \dots, n/2\}$  for the encoder pre-training and  $\mathcal{D}_2 = \mathcal{D} \setminus \mathcal{D}_1$  for the later fusion training.

The low-resolution encoder  $E_l$  is trained to regress the high-resolution encodings  $z_i = E_h(x_i^h)$  from  $x_i^l$ , while also preserving the super-resolution constraint, i.e., that the downsampled generated image matches the low-resolution input image. By combining these constraints, we minimize

$$\min_{E_l} \sum_{x_i^l, x_i^h \in \mathcal{D}_1} |E_l(x_i^l) - E_h(x_i^h)|_1 + \lambda |D \circ G(E_l(x_i^l)) - x_i^l|_2^2, \quad (2)$$

where  $D \circ x$  is the downsampling of  $x$  and  $\lambda = 40$ . In the case of the audio encoding, regressing all the information in  $z_i$  with  $E_a(a_i)$  is not possible, as many of the factors of variation in  $z_i$ , e.g., the

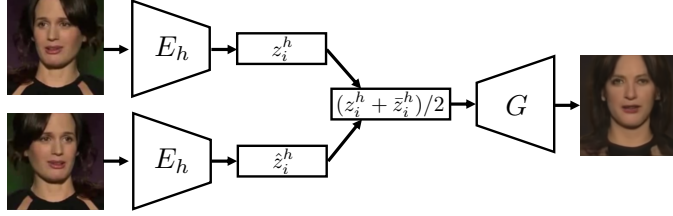


Figure 2: Illustration of how we compute the targets for the audio encoder pre-training. We feed a high-resolution training image and its horizontally flipped version through the high-resolution encoder. The resulting latent codes are then averaged and used as targets. The averaged latent code produces a face in neutral frontal facing pose.

pose of the face, are not present in  $a_i$ . To remove the pose from  $z_i$  we generate the targets for the audio encoder as  $\bar{z}_i = \frac{1}{2}(E_h(x_i^h) + E_h(\hat{x}_i^h))$ , where  $\hat{x}_i^h$  is a horizontally flipped version of the image  $x_i^h$ . As it turns out, due to the disentangled representations of  $G$ , the reconstruction  $G(\bar{z}_i)$  produces a neutral frontal facing version of  $G(z_i)$  (see Fig. 2). The audio encoder  $E_a$  is finally trained to minimize

$$\min_{E_a} \sum_{a_i, x_i^h \in \mathcal{D}_1} |E_a(a_i) - \bar{z}_i|_1. \quad (3)$$

### 3.4 Fusing Audio and Low-Resolution Encodings

Given the pre-trained encoders  $E_l$  and  $E_a$ , we now want to fuse the information provided by the two signals. Since the low-resolution encoder  $E_l$  already provides a good approximation to  $E_h$  it is reasonable to use it as a starting point for the final prediction. Conceptually, we can think of  $E_l$  as providing a  $z_i^l = E_l(x_i^l)$  that results in a canonical face  $G(z_i^l)$  corresponding to the low-resolution image  $x_i^l$ . Ambiguities in  $z_i^l$  could then possibly be resolved via the use of the audio, which would provide an estimate of the residual  $\Delta z_i = z_i - z_i^l$ . We therefore model the fusion mechanism as  $z_i^f = E_l(x_i^l) + F(E_l(x_i^l), E_a(a_i))$ , where  $F$  is a simple fully-connected network acting on the concatenation of  $E_l(x_i^l)$  and  $E_a(a_i)$ . Since the audio-encoding  $E_a$  might be suboptimal for the fusion, we continue training it along with  $F$ . The limited complexity of the function  $F$  prevents the overfitting to the low-resolution encoding, but provides the necessary context for the computation of  $\Delta z_i$ . To summarize, we train the fusion by optimizing

$$\min_{E_a, F} \sum_{a_i, x_i^h, x_i^l \in \mathcal{D}_2} |z_i^l + F(z_i^l, E_a(a_i)) - z_i|_1 + |D \circ G(z_i^l + F(z_i^l, E_a(a_i))) - x_i^l|_2^2. \quad (4)$$

## 4 Experiments

### 4.1 Dataset

We performed all our experiments on a subset of the VoxCeleb2 dataset (Chung et al. [2018]). The dataset contains over one million audio tracks extracted from 145K videos of people speaking. For the full training set  $\mathcal{D}$  we selected 104K videos with 545K audio tracks and extracted around 2M  $128 \times 128$  frames such that each speaker has at least 500 associated frames. We then split this dataset in half to create  $\mathcal{D}_1$  and  $\mathcal{D}_2$  in such a way that  $\mathcal{D}_1$  and  $\mathcal{D}_2$  contain the same speakers but different videos. For the test set we selected 39K frames and 37K utterances from 25K videos not contained in the training set (again from the same speakers). In the end we select around 4K speakers out of the 6K speakers in the full dataset (filtering out speakers with very few videos and audio tracks). Note that this selection is purely done to allow the evaluation via a speaker identity classifier.

### 4.2 Implementation

The style-based generator  $G$  was pre-trained on the full training set  $\mathcal{D}$  with all hyper-parameters set to their default values (see Karras et al. [2018] for details). It has seen a total of 31 million images. The

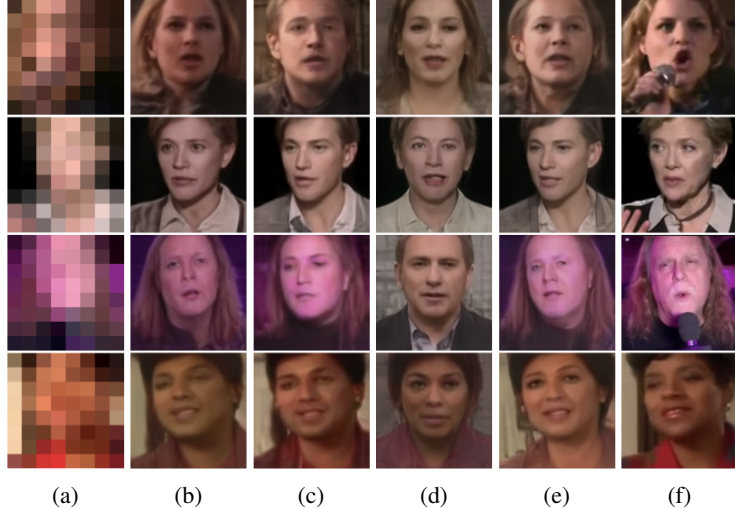


Figure 3: We show selected examples of reconstructions to some of our ablation experiments. The  $8 \times 8$  pixels low-resolution inputs are shown in (a) and the corresponding  $128 \times 128$  pixels ground truth images are shown in column (f). In-between, we show results for  $E_h$  in (b),  $E_l$  in (c),  $E_a$  in (d) and our fusion model  $F$  with fine-tuned  $E_a$  in (e).

high-resolution encoder  $E_h$  was trained for 125K iterations and a batch-size of 256 on the  $128 \times 128$  pixels images from  $\mathcal{D}$ . The low-resolution encoder  $E_l$  and the audio encoder  $E_a$  were trained on  $\mathcal{D}_1$ .  $E_l$  was trained for 45K iterations with a batch-size of 256 and  $E_a$  was trained for 95K iterations and a batch-size of 128. The inputs  $x_i^l$  to  $E_l$  are of size  $8 \times 8$  pixels and the inputs to  $E_a$  are the audio log-spectrograms of  $a_i$  of size  $257 \times 257$  elements. The fine-tuning of  $E_a$  and the training of the fusion layer  $F$  was performed for 115K iterations on  $\mathcal{D}_2$ . We used the Adam optimizer (Kingma and Ba [2014]) with a fixed learning rate of  $10^{-4}$  for the training of all the networks. A detailed description of the network architectures can be found in the supplementary material.

### 4.3 Gender and Identity Classification Accuracy as a Performance Measure

To evaluate the capability of our model to recover gender and other identity attributes based on the low-resolution and audio inputs we propose to use the accuracy of a pre-trained identity classifier  $C_i$  and gender classifier  $C_g$ . To this end, we fine-tune two VGG-Face CNNs of Parkhi et al. [2015] on the training set  $\mathcal{D}$  for 10 epochs on both face attributes. As you can see in Table 1 these classifiers perform well on the test set on both face attributes.

**Ablations.** We performed ablation experiments to understand the information retained in the encoders and to justify the design of our final model. The accuracy of the classifiers  $C_i$  and  $C_g$  are reported in Table 1 for the following ablation experiments:

- (a)-(c) Individual components:** Shows the performance of the individual encoders on their own. Results for the high-resolution encoder  $E_h$ , the low-resolution encoder  $E_l$  and the audio encoder  $E_a$  are reported.
- (d)-(f) Fusion strategies:** The performance of different fusion strategies is reported. We report results of our fusion model  $F$  with a single fully-connected layer and fine-tuning of  $E_a$ . We compare this to results of a more complex fusion network  $F_3$  with three fully-connected layers and a version of  $F$  without fine-tuning of  $E_a$ .

We can observe that  $E_a$  is able to predict the correct gender more often than  $E_l$ . All the fusion approaches lead to an improvement in terms of identity prediction over  $E_a$  and  $E_l$  alone, thus showing that the information from both inputs is successfully integrated. Note that the limited performance of  $E_h$  might be due to some degree of mode-collapse in  $G$  and the resulting inability of  $G$  to exactly reconstruct all the high resolution images. See Fig. 3 for qualitative results.

Table 1: Results of our ablation experiments. We report the accuracy of an identity classifier  $C_i$  and a gender classifier  $C_g$  on generated high-resolution images.

Ablation	Accuracy $C_i$	Accuracy $C_g$
High-resolution test images	95.25%	99.53%
(a) $E_h$ only	34.31%	95.60%
(b) $E_i$ only	11.23%	91.89%
(c) $E_a$ only	10.12%	95.71%
(d) $F$ + fine-tuned $E_a$	16.99%	93.92%
(e) $F_3$ + fine-tuned $E_a$	20.96%	95.03%
(f) $F$ + fixed $E_a$	11.54%	92.44%

Table 2: Comparison to other general-purpose super-resolution methods at different super-resolution factors. We report PSNR and SSIM obtained on the test set. Note that the target resolution is fixed at  $128 \times 128$  pixels and therefore the inputs to the  $4\times$  methods is  $32 \times 32$  pixels while our model only uses  $8 \times 8$  pixels input images.

Method	Factor	PSNR	SSIM	Accuracy $C_i$	Accuracy $C_g$
SRGAN (Ledig et al. [2017])	$4\times$	26.21	0.85	52.95%	97.01%
VDSR (Kim et al. [2016])	$4\times$	25.47	0.85	89.61%	99.02%
SRFeat (Park et al. [2018])	$4\times$	27.02	0.83	93.40%	99.27%
LapSRN (Lai et al. [2017])	$4\times$	31.99	0.91	93.83%	99.38%
Bicubic	$16\times$	17.93	0.49	0.10%	59.67%
LapSRN (Lai et al. [2017])	$16\times$	22.75	0.64	5.27%	83.27%
Ours $F$	$16\times$	19.15	0.57	16.99%	93.92%
Ours $F_3$	$16\times$	19.74	0.57	20.96%	95.03%

**Comparisons to Other Super-Resolution Methods.** We compare to state-of-the-art super-resolution methods in Table 2 and Fig. 4. The standard metrics PSNR and SSIM along with the accuracy of  $C_i$  and  $C_g$  are reported for super-resolved images of our test set. Note that most other methods were not trained on extreme super-resolution factors of  $16\times$ , but rather on factors of  $4\times$ . Unsurprisingly, the methods using a factor of  $4\times$  perform much better than our model in terms of PSNR and SSIM. Notice that although LapSRN trained on  $16\times$  super-resolution performs better in terms of PSNR and SSIM than our method, the quality of the recovered image is clearly worse (see Fig. 4). This difference in the quality is instead revealed by evaluating the gender and identity classification accuracies of the restored images. This suggests that while PSNR and SSIM may be suitable metrics to evaluate reconstructions with small super-resolution factors, they may not be suitable to assess the reconstructions in more extreme cases such as with a factor of  $16\times$ .

**Editing by Mixing Audio Sources.** Our model allows us to influence the high-resolution output by interchanging the audio track used in the fusion. To demonstrate this capability we show examples where we mix a fixed low-resolution input with several different audio sources in Fig. 5. We also use this mixing modality to show quantitatively that audio is used in the generation of the high-resolution image. We generate 18,864 high-resolution images by taking low-resolution images and audios from videos of persons of different gender. We then classify the gender of these high-resolution images and find that in 29.41% of the cases the predicted gender matched that of the audio source.

## 5 Conclusions

We have introduced a new paradigm for face super-resolution, where also audio contributes to the restoration of missing details in the low-resolution input image. We have described the design of a neural network and the corresponding training procedure to successfully make use of the audio signal despite the difficulty of extracting visual information from it. We have also shown quantitatively that audio can contribute to improving the accuracy of the identity as well as the gender of the restored face. Moreover, we have shown that it is possible to mix low-resolution images and audios from different videos and obtain semantically meaningful high resolution images.

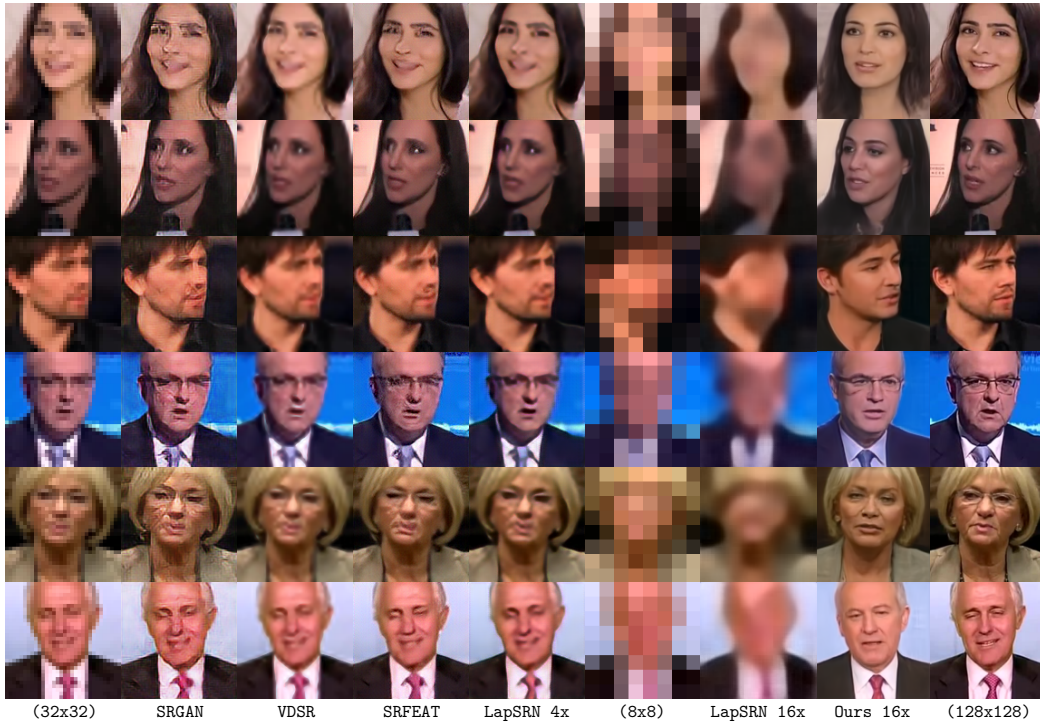


Figure 4: We compare to other super-resolution methods on our test set. The first column shows the  $32 \times 32$  pixels inputs for prior super-resolution works. Columns 2 to 5 show results for SRGAN, VDSR, SRFEAT and LapSRN. Column 6 shows the  $8 \times 8$  pixels inputs and the output of LapSRN and of our model are shown in column 7 and 8. The ground-truth high-resolution image is shown in the last column.



Figure 5: We show examples where we mix a given low-resolution image with different audio sources. The top row shows the high-resolution images from which we take the audio track. The first two columns on the left show the same high-resolution images and the corresponding low-resolution images used as input. The rest of the images in the matrix are generated by mixing the low-res from a row with the audio of a column.

## References

- Namhyuk Ahn, Byungkon Kang, and Kyung-Ah Sohn. Fast, accurate, and lightweight super-resolution with cascading residual network. In *The European Conference on Computer Vision (ECCV)*, September 2018.
- Relja Arandjelovic and Andrew Zisserman. Objects that sound. In *The European Conference on Computer Vision (ECCV)*, September 2018.
- Adrian Bulat and Georgios Tzimiropoulos. Super-fan: Integrated facial landmark localization and super-resolution of real-world low resolution faces in arbitrary poses with gans. In *The IEEE Conference on Computer Vision and Pattern Recognition (CVPR)*, June 2018.
- Adrian Bulat, Jing Yang, and Georgios Tzimiropoulos. To learn image super-resolution, use a gan to learn how to do image degradation first. In *The European Conference on Computer Vision (ECCV)*, September 2018.
- Yu Chen, Ying Tai, Xiaoming Liu, Chunhua Shen, and Jian Yang. Fsrnet: End-to-end learning face super-resolution with facial priors. In *The IEEE Conference on Computer Vision and Pattern Recognition (CVPR)*, June 2018.
- J. S. Chung, A. Nagrani, and A. Zisserman. Voxceleb2: Deep speaker recognition. In *INTERSPEECH*, 2018.
- A. Ephrat, I. Mosseri, O. Lang, T. Dekel, K Wilson, A. Hassidim, W. T. Freeman, and M. Rubinstein. Looking to listen at the cocktail party: A speaker-independent audio-visual model for speech separation. *arXiv preprint arXiv:1804.03619*, 2018.
- Ruohan Gao, Rogerio Feris, and Kristen Grauman. Learning to separate object sounds by watching unlabeled video. In *The European Conference on Computer Vision (ECCV)*, September 2018.
- Wei Han, Shiyu Chang, Ding Liu, Mo Yu, Michael Witbrock, and Thomas S. Huang. Image super-resolution via dual-state recurrent networks. In *The IEEE Conference on Computer Vision and Pattern Recognition (CVPR)*, June 2018.
- Muhammad Haris, Gregory Shakhnarovich, and Norimichi Ukita. Deep back-projection networks for super-resolution. In *The IEEE Conference on Computer Vision and Pattern Recognition (CVPR)*, June 2018.
- Zheng Hui, Xiumei Wang, and Xinbo Gao. Fast and accurate single image super-resolution via information distillation network. In *The IEEE Conference on Computer Vision and Pattern Recognition (CVPR)*, June 2018.
- Tero Karras, Samuli Laine, and Timo Aila. A style-based generator architecture for generative adversarial networks. *arXiv preprint arXiv:1812.04948*, 2018.
- Jiwon Kim, Jung Kwon Lee, and Kyoung Mu Lee. Accurate image super-resolution using very deep convolutional networks. In *Proceedings of the IEEE conference on computer vision and pattern recognition*, pages 1646–1654, 2016.
- Diederik P Kingma and Jimmy Ba. Adam: A method for stochastic optimization. *arXiv preprint arXiv:1412.6980*, 2014.
- Wei-Sheng Lai, Jia-Bin Huang, Narendra Ahuja, and Ming-Hsuan Yang. Deep laplacian pyramid networks for fast and accurate super-resolution. In *The IEEE Conference on Computer Vision and Pattern Recognition (CVPR)*, July 2017.
- Christian Ledig, Lucas Theis, Ferenc Huszar, Jose Caballero, Andrew Cunningham, Alejandro Acosta, Andrew Aitken, Alykhan Tejani, Johannes Totz, Zehan Wang, and Wenzhe Shi. Photo-realistic single image super-resolution using a generative adversarial network. In *The IEEE Conference on Computer Vision and Pattern Recognition (CVPR)*, July 2017.
- Juncheng Li, Faming Fang, Kangfu Mei, and Guixu Zhang. Multi-scale residual network for image super-resolution. In *The European Conference on Computer Vision (ECCV)*, September 2018.
- Andrew Owens and Alexei A. Efros. Audio-visual scene analysis with self-supervised multisensory features. In *The European Conference on Computer Vision (ECCV)*, September 2018.
- Seong-Jin Park, Hyeonseok Son, Sunghyun Cho, Ki-Sang Hong, and Seungyong Lee. Srfeat: Single image super-resolution with feature discrimination. In *The European Conference on Computer Vision (ECCV)*, September 2018.
- O. M. Parkhi, A. Vedaldi, and A. Zisserman. Deep face recognition. In *British Machine Vision Conference*, 2015.

- Eli Shlizerman, Lucio Dery, Hayden Schoen, and Ira Kemelmacher-Shlizerman. Audio to body dynamics. In *The IEEE Conference on Computer Vision and Pattern Recognition (CVPR)*, June 2018.
- Harriet M J Smith, Andrew K Dunn, Thom Baguley, and Paula C Stacey. Matching novel face and voice identity using static and dynamic facial images. *Attention, perception & psychophysics*, 78(3):868–879, 2016.
- Yang Song, Jingwen Zhu, Xiaolong Wang, and Hairong Qi. Talking face generation by conditional recurrent adversarial network. *arXiv preprint arXiv:1804.04786*, 2018.
- Auston Sterling, Justin Wilson, Sam Lowe, and Ming C. Lin. Isnn: Impact sound neural network for audio-visual object classification. In *The European Conference on Computer Vision (ECCV)*, September 2018.
- Ying Tai, Jian Yang, and Xiaoming Liu. Image super-resolution via deep recursive residual network. In *The IEEE Conference on Computer Vision and Pattern Recognition (CVPR)*, July 2017.
- Yapeng Tian, Jing Shi, Bochen Li, Zhiyao Duan, and Chenliang Xu. Audio-visual event localization in unconstrained videos. In *The European Conference on Computer Vision (ECCV)*, September 2018.
- Xintao Wang, Ke Yu, Chao Dong, and Chen Change Loy. Recovering realistic texture in image super-resolution by deep spatial feature transform. In *The IEEE Conference on Computer Vision and Pattern Recognition (CVPR)*, June 2018.
- Xiangyu Xu, Deqing Sun, Jinshan Pan, Yujin Zhang, Hanspeter Pfister, and Ming-Hsuan Yang. Learning to super-resolve blurry face and text images. In *The IEEE International Conference on Computer Vision (ICCV)*, Oct 2017.
- Xin Yu, Basura Fernando, Bernard Ghanem, Fatih Porikli, and Richard Hartley. Face super-resolution guided by facial component heatmaps. In *The European Conference on Computer Vision (ECCV)*, September 2018a.
- Xin Yu, Basura Fernando, Richard Hartley, and Fatih Porikli. Super-resolving very low-resolution face images with supplementary attributes. In *The IEEE Conference on Computer Vision and Pattern Recognition (CVPR)*, June 2018b.
- Kaipeng Zhang, Zhanpeng Zhang, Chia-Wen Cheng, Winston H. Hsu, Yu Qiao, Wei Liu, and Tong Zhang. Super-identity convolutional neural network for face hallucination. In *The European Conference on Computer Vision (ECCV)*, September 2018a.
- Yulun Zhang, Kunpeng Li, Kai Li, Lichen Wang, Bineng Zhong, and Yun Fu. Image super-resolution using very deep residual channel attention networks. In *The European Conference on Computer Vision (ECCV)*, September 2018b.
- Yulun Zhang, Yapeng Tian, Yu Kong, Bineng Zhong, and Yun Fu. Residual dense network for image super-resolution. In *The IEEE Conference on Computer Vision and Pattern Recognition (CVPR)*, June 2018c.
- Hang Zhao, Chuang Gan, Andrew Rouditchenko, Carl Vondrick, Josh McDermott, and Antonio Torralba. The sound of pixels. In *The European Conference on Computer Vision (ECCV)*, September 2018.
- Yipin Zhou, Zhaowen Wang, Chen Fang, Trung Bui, and Tamara L. Berg. Visual to sound: Generating natural sound for videos in the wild. In *The IEEE Conference on Computer Vision and Pattern Recognition (CVPR)*, June 2018.
- Hao Zhu, Aihua Zheng, Huaibo Huang, and Ran He. High-resolution talking face generation via mutual information approximation. *arXiv preprint arXiv:1812.06589*, 2018.